A 3DVAR-Based Dynamical Initialization Scheme for Tropical Cyclone Predictions*

SHENGJUN ZHANG

State Key Laboratory of Severe Weather, Chinese Academy of Meteorological Sciences, Beijing, China

TIM LI AND XUYANG GE

International Pacific Research Center, University of Hawaii at Manoa, Honolulu, Hawaii

MELINDA PENG

Naval Research Laboratory, Monterey, California

NING PAN

Fujian Meteorological Bureau, Fuzhou, Fujian, China

(Manuscript received 17 December 2010, in final form 3 November 2011)

ABSTRACT

A combined tropical cyclone dynamic initialization–three-dimensional variational data assimilation scheme (TCDI–3DVAR) is proposed. The specific procedure for the new initialization scheme is described as follows. First, a first-guess vortex field derived from a global analysis will be spun up in a full-physics mesoscale regional model in a quiescent environment. During the spinup period, the weak vortex is forced toward the observed central minimum sea level pressure (MSLP). The so-generated balanced TC vortex with realistic MSLP and a warm core is then merged into the environmental field and used in the subsequent 3DVAR data assimilation. The observation system simulation experiments (OSSEs) demonstrate that this new TC initialization scheme leads to much improved initial MSLP, warm core, and asymmetric temperature patterns compared to those from the conventional 3DVAR scheme. Forecasts of TC intensity with the new initialization scheme are made, and the results show that the new scheme is able to predict the ''observed'' TC intensity change, compared to runs with the conventional 3DVAR scheme or the TCDI-only scheme. Sensitivity experiments further show that the intensity forecasts with knowledge of the initial MSLP and wind fields appear more skillful than do the cases where the initial MSLP, temperature, and humidity fields are known. The numerical experiments above demonstrate the potential usefulness of the proposed new initialization scheme in operational applications. A preliminary test of this scheme with a navy operational model shows encouraging results.

1. Introduction

While tropical cyclone (TC) track forecasts have been steadily improved during the past decades due to the improved resolution and physics of numerical weather prediction (NWP) models and the increased usage of unconventional observations such as satellite radiance (McAdie and Lawrence 2000), the skill of predicting TC intensity change remains low (DeMaria and Kaplan 1999; Knaff et al. 2005; DeMaria et al. 2005), and it is a great challenge to the TC community. Among many causes of the low TC intensity forecast skill, the poor representation of initial TCs in the operational NWP models is probably one of the most important factors.

Efforts have made in the past to improve TC initial conditions in NWP models. A common method for TC initialization is to first construct a synthetic vortex using the officially estimated parameters such as minimum central

* School of Ocean and Earth Science and Technology Contribution Number 8563 and International Pacific Research Center Contribution Number 855.

Corresponding author address: Tim Li, IPRC, University of Hawaii, 1680 East–West Rd., Honolulu, HI 96822.
E-mail: timli@hawaii.edu

DOI: 10.1175/WAF-D-10-05066.1

sea level pressure, maximum wind speed, and/or the size of the TC and then implant the synthetic vortex into the environmental flow (e.g., Ueno 1989; Kurihara et al. 1993; Leslie and Holland 1995; Nuissier et al. 2005). Kurihara et al. (1993) developed a sophisticated filtering scheme to remove the often erroneous first-guess vortex prior to the implantation of a synthetic vortex. Zou and Xiao (2000) and Xiao et al. (2000, 2009) developed a four-dimensional variational (4DVAR) bogus data assimilation (BDA) technique with a fixed empirical surface pressure profile.

Two major U.S. operational TC forecast systems at the Naval Research Laboratory/Fleet Numerical Meteorology and Oceanography Center (NRL/FNMOC) and the National Centers for Environmental Prediction (NCEP) apply different TC initialization schemes, respectively. The Navy Operational Global Atmosphere Prediction System (NOGAPS) includes synthetic data to represent TC vortices treated as convectional dropsonde data, while the NCEP Global Forecast System (GFS) uses a relocation method without adding synthetic data. Regardless of the differences in the initial wind fields of TCs between the two operational forecast systems, both have a much weaker initial TC MSLP compared to what is observed. For instance, for Atlantic Hurricane Francis (2004) (which caused devastating damage in Florida), when the observed MSLP reached 940 hPa on 1 September, the NCEP analysis had a minimum pressure of 998 hPa whereas the NOGAPS analysis showed an MSLP of 992 hPa. Given such a large bias in the initial MSLP, it is anticipated that the TC intensity forecast error in the forecast would be quite large.

It is worth mentioning that during the update data assimilation cycle, the initial TC MSLP was provided by the best-track information into the operational 3DVAR assimilation systems for both models. Why is the current 3DVAR system incapable of preserving the observed MSLP information? In this study, we intend to explore this problem through a series of observation system simulation experiments (OSSEs), using the Advanced Research Weather Research and Forecast Model (WRF-ARW; Michalakes et al. 1999; Skamarock et al. 2005), and its 3DVAR system (Barker et al. 2004a,b). This part of the study is given in section 2. A new method, a 3DVAR-based dynamical TC initialization scheme, is introduced in section 3 to overcome the current problem. As demonstrated, the resulted TC initial conditions, including symmetric and asymmetric components, is close to the ''observed'' state. The forecasts of the TC intensity evolution with or without the improved TC initial conditions are described in section 4. A discussion of the background-error covariance matrix (hereafter BE), observation error covariance matrix, and a brief description of the application of the current tropical cyclone dynamic initialization (TCDI)–3DVAR scheme in real-case operational forecasts are given in section 5. Finally, a summary is given in section 6.

2. Observation system simulation experiments with conventional 3DVAR assimilation

In this section, we conducted an observation system simulation experiment (OSSE) study using the WRF and its 3DVAR system. The OSSE assumes a perfect model scenario, which provides an idealized framework for evaluating the performance of the current data assimilation system in TC initializations in most models. Using the model-generated TC as the ''observation,'' we avoid two practical problems in the real environment: 1) limited observations in both dynamic (wind) and thermodynamic (pressure, temperature, and humidity) fields for TCs and 2) interpolation errors from the observational positions to model grids.

The WRF used has a uniform grid size of 30 km. The domain consists of 151 × 151 grid points, covering an area of 4500 km × 4500 km, with 27 levels in the vertical. The Kain–Fritch convective scheme (Kain and Fritsch, 1990) and Lin microphysics scheme (Lin et al. 1983) are used. The PBL scheme follows that of Hong et al. (2006), which is a modified version of the Medium-Range Forecast Model (MRF) scheme of Hong and Pan (1996). Both longwave and shortwave radiation processes are included in the simulations. A fixed lateral boundary condition is applied; that is, the tendency of prognostic variables in the lateral boundary is set to zero.

We specify a weak initial balanced axisymmetric vortex with a wind profile as follows:

$$V_t(r,\sigma) = A(\sigma)\frac{3\sqrt{6}}{4}V_m\left(\frac{r}{r_m}\right)\left[1+\frac{1}{2}\left(\frac{r}{r_m}\right)^2\right]^{-3/2}, \quad (1)$$

where r is the radial distance from the vortex center, V_m is the maximum tangential wind at the radius of r_m, σ is vertical sigma levels, and $A(\sigma)$ specifies the vertical structure. Given the wind fields, the mass and thermodynamic fields are then obtained based on a nonlinear balance equation so that the initial vortex satisfies both the hydrostatic and gradient wind balances (Wang 2001). Figure 1 shows the temperature and tangential wind profiles of this initially weak vortex specified in the model. A maximum 850-hPa wind speed of 14 m s^{-1} appears at a radius of 100 km. This corresponds to a 1.5-K warm core at 600 hPa according to a thermal wind relation. The initial water vapor mixing ratio and other thermodynamic variables are assumed to be horizontally homogeneous and have the vertical profiles of typical January mean observations at Willis Island, northeast of Australia

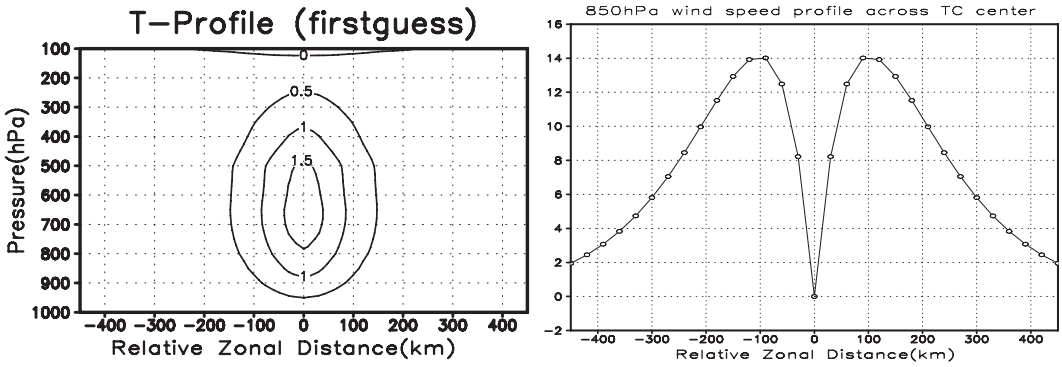

FIG. 1. (left) Zonal–vertical cross section of the temperature anomaly (deviated from the level-mean temperature, K) and (right) east–west cross section across the vortex center of 850-hPa wind speed (m s^{-1}) from the first-guess initial bogus field. The horizontal axis is the relative zonal distance (km) to the vortex center.

(Holland 1997). Other model parameter settings are identical to those described in Zhou and Wang (2009). The model is set on an *f* plane centered at 15°N, and a quiescent environment with a constant sea surface temperature (SST) of 29°C is specified.

At the end of the 48-h integration, a three-dimensional (3D) TC structure, with an MSLP of about 980 hPa, is obtained. Figure 2 shows the model-simulated lower- and upper-level wind fields, along with the zonal–vertical cross sections of perturbation temperature (with the mean value at each level removed), zonal and meridional wind components, and geopotential height. While the 850-hPa flow is featured by cyclonic inflows, the wind at 200 hPa in the outer region is dominated by anticyclonic outflows. The vertical temperature profile shows a clear warm core in the mid- to upper troposphere, with an anomalous warm temperature of about 5 K at 250 hPa. The geopotential height shows a strong negative center in the low levels. The zonal and meridional winds in the cross section may be approximately regarded as radial and tangential flow components. A deep cyclonic layer is accompanied by a strong inflow in the planetary boundary layer.

As shown in Fig. 2, the WRF simulates a mature TC structure with the warm core, the inflow at the lower level, and the outflow at the upper level. The purpose of the OSSE in this section is to evaluate the ability of the conventional 3DVAR scheme in reproducing the TC dynamic and thermodynamic fields. To achieve this goal, the gridpoint data from this simulated vortex are treated as the observed data. We use the initial weak vortex with 1002-hPa central pressure (Fig. 1) as the first guess, and an observation error covariance matrix stored in the original WRF 3DVAR code was applied.

Figure 3 shows the results after the WRF conventional 3DVAR assimilation. Comparing with the ''observations'' (Fig. 2), we note that the winds are in general well assimilated. For the temperature profile, however, both the pattern and amplitude of the warm core have serious errors. The warm core in the upper level is less than a half of the observed magnitude, and the warm core is split into two centers, one in the upper troposphere at 250 hPa and the other in the lower troposphere around 800 hPa. The assimilated geopotential height also is much weaker. Accompanying the large temperature and geopotential biases is the much weaker sea level pressure (Fig. 4). The assimilated MSLP is 1000 hPa, which is very close to the first-guess value provided.

The OSSE results above indicate that given a weak vortex as the first guess with the knowledge of observed 3D TC fields, the conventional 3DVAR assimilation is capable of retrieving the momentum fields (such as the TC tangential and radial wind) very well, but is unable to recover the observed thermodynamic fields such as temperature, geopotential height, and surface pressure fields. Both the TC MSLP and warm core are severely underestimated. Such a failure of TC initialization greatly affects the subsequent TC intensity forecast in the operational models. Thus, it is necessary to develop a new initialization strategy to overcome the aforementioned problem.

3. A combined 3DVAR and dynamic initialization scheme

Why does the WRF 3DVAR ''reject'' the observed MSLP and other thermodynamic field information in the TC initialization procedure? An examination of the WRF 3DVAR code indicates that a transfer from standard pressure level fields to those in a sigma vertical coordinate without the knowledge of the actual TC central minimum pressure value is the part of the problem. For example, in some strong typhoon cases the differences between the observed MSLP and first guess MSLP can be as large as 50 hPa. Such a difference may lead to significant large biases in the dynamic and thermodynamic

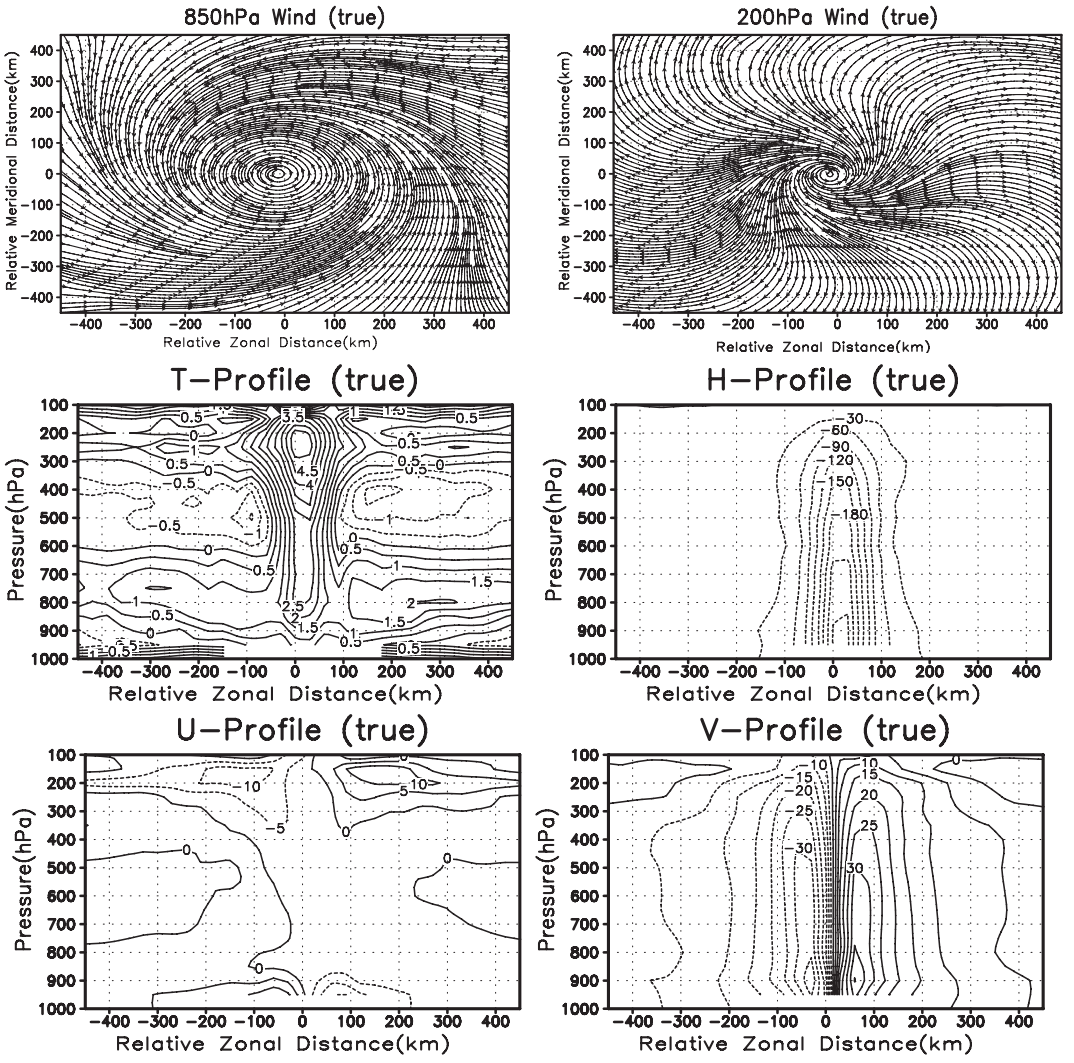

FIG. 2. WRF-simulated (top) 850- and 200-hPa streamlines and (middle) zonal–vertical cross sections of temperature and geopotential height anomalies (departure from the level mean values; K and m, respectively), and (bottom) zonal and meridional wind components (m s^{-1}) across the TC center at hour 48. This TC state is regarded as the "observation" in the subsequent 3DVAR assimilation.

fields near the TC core. In addition, an application of a general geostrophic wind–pressure relation in the 3DVAR constraint is another possible cause. Furthermore, uncertainty in the background and observation error covariance is also a possible cause, which will be discussed in section 5.

Our strategy in the new TC initialization scheme is to improve the first-guess field prior to 3DVAR so that the errors associated with the pressure-to-sigma coordinate transfer can be minimized. Based on the findings and consideration mentioned above, we have developed a TCDI scheme. The TCDI package consists of a primitive equation system with full nonlinear dynamics and physics. Prior to TCDI, the first-guess field is decomposed into a TC vortex and its environmental field, following Kurihara et al. (1993). Then, we integrate the third version of the Tropical Cyclone Model (TCM3; Wang 2001) with the decomposed TC vortex as an initial condition. During the integration, the weak vortex is forced toward the observed MSLP by adding a Newtonian damping (restoring) term in the surface pressure tendency equation; that is,

$$\frac{dp}{dt} = -\alpha(P - P_{\text{obs}}), \tag{2}$$

where P_{obs} denotes the observed MSLP and α is a relaxation coefficient ($8 \times 10^{-3} \cdot s^{-1}$), which corresponds to a reversed time scale of 12 h.

In addition, to assimilate the asymmetric heating effect, a 3D asymmetric heating field [derived from either

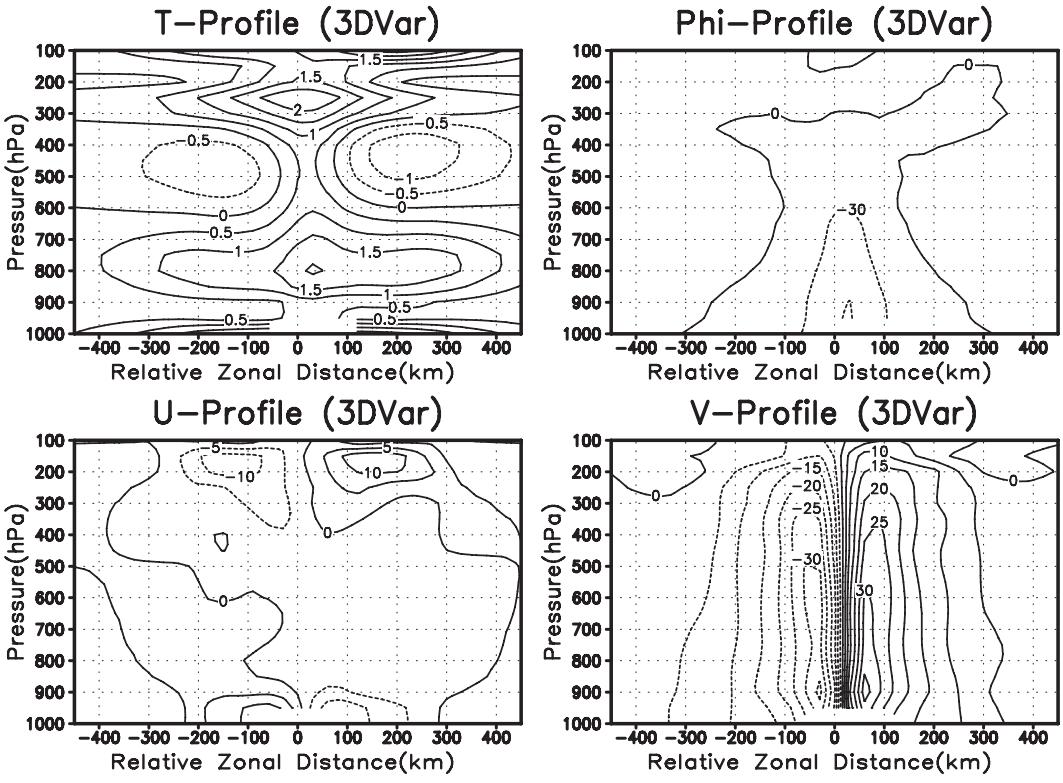

FIG. 3. (top) Zonal–vertical cross sections of temperature and geopotential height anomalies (K and m, respectively) and (bottom) zonal and meridional winds (m s^{-1}) across the TC center, after the 3DVAR assimilation.

the model output from the OSSE experiment or from the Tropical Rainfall Measuring Mission (TRMM) rain rate field] may be specified in the thermodynamic equation.

In a previous study (e.g., Zou and Xiao 2000), a two-dimensional (2D) surface pressure field with an empirical radial distribution is used as the nudging field. The disadvantage of this approach is that the near-surface wind is fixed and cannot evolve freely. By forcing only the central pressure toward the observed MSLP following Zhang et al. (2007), we allow the TC momentum fields to be adjusted freely without constraint on its horizontal pattern, so that the observed heating field may help generate asymmetric TC flows. This approach is practical as TRMM Microwave Imager (TMI) and Special Sensor Microwave Imager/Sounder (SSMI/S) products provide high-resolution 2D or 3D rain-rate fields. The current approach may potentially derive both symmetric and asymmetric initial TC fields.

The following is a specific procedure for the combined TCDI–3DVAR scheme. First, a specified Rankine vortex or a vortex extracted from a global analysis field will be spun up in a model with full nonlinear dynamics and physics in a quiescent environment. During the spinup period, the weak vortex is forced toward the observed MSLP with a 3D heating field imposed. The final product is a balanced TC vortex with a realistic MSLP and warm core. The balanced TC vortex is then inserted into the environmental field and the total field is used as the first guess in the subsequent 3DVAR assimilation.

Figure 5 depicts the results after the combined TCDI–3DVAR assimilation. Both the dynamic and thermodynamic fields are now very close to the observations (Fig. 2). For example, the amplitude of the warm core in

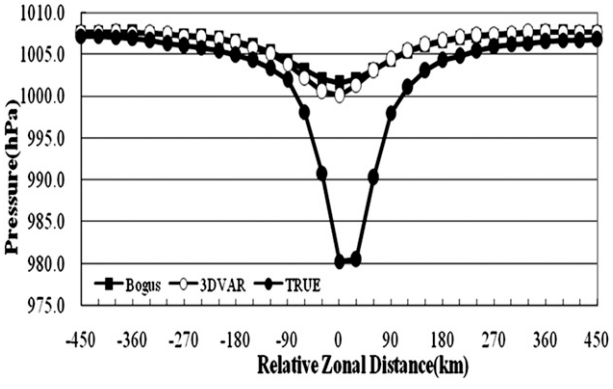

FIG. 4. Zonal profiles of the surface pressure across the vortex center derived from the first-guess bogus field (filled squares), the conventional 3DVAR assimilation (open circles), and the observations (filled circles).

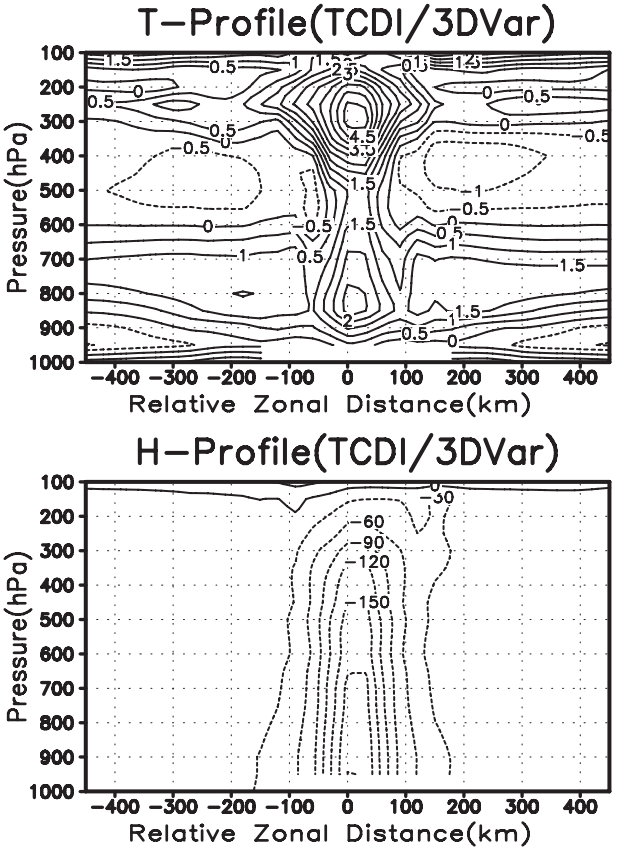

FIG. 5. Zonal–vertical cross sections of (top) assimilated temperature (K) and (bottom) geopotential height (m) anomalies derived from the combined TCDI–3DVAR scheme.

the upper troposphere is 5 K. The geopotential height field shows a strong negative column, resembling the observed pattern.

Comparing to Fig. 2, a marked difference appears in the assimilated surface pressure field using the new approach, as shown in Fig. 6. The assimilated MSLP is now 983 hPa, much closer to the observed MSLP value. The result indicates that the combined TCDI–3DVAR initialization scheme significantly improves the initial TC intensity and thermodynamic structure, compared to the conventional 3DVAR scheme (Fig. 4).

To demonstrate that the new scheme improves not only the symmetric component of the TC fields but also the asymmetric component, we conducted an additional OSSE experiment in which we use an asymmetric TC vortex as the observed TC state. It was generated by inserting an asymmetric heating field during the model integration when spinning up the vortex. Through this idealized experiment, we examine how well the new initialization scheme captures TC asymmetric flow and temperature patterns. Figure 7 shows the horizontal patterns of the observed wind speed field at 850 hPa and its counterpart

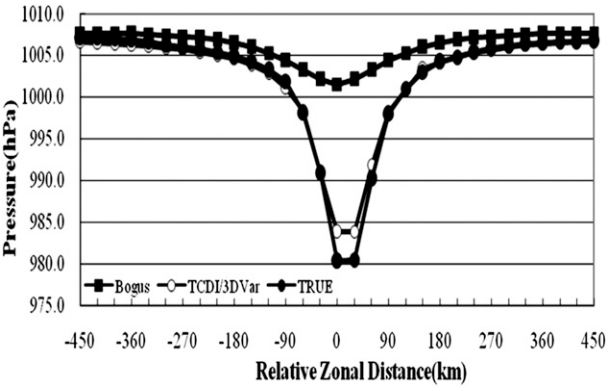

FIG. 6. Zonal profiles of the surface pressure across the vortex center derived from the first-guess bogus field (filled squares), the combined TCDI–3DVAR assimilation scheme (open circles), and the observations (filled circles).

from the conventional 3DVAR and TCDI–3DVAR assimilations. At 850 hPa, the observed maximum wind speed is located in the northwest quadrant. The assimilated 850-hPa wind speed field has the same feature as the observations. In addition to the asymmetry pattern, the amplitude of the wind asymmetry is also close to the observations. It is noted that the conventional 3DVAR scheme captures a similar asymmetric wind structure.

Next, we examine the assimilated asymmetric temperature fields. Figure 8 shows the wavenumber-1 asymmetric component of the perturbation temperature fields at 500 hPa from the observed and the assimilated fields. A positive temperature center is found in the southwest quadrant at 500 hPa in the observed field. Such an asymmetric pattern is well captured by both the TCDI–3DVAR and the conventional 3DVAR schemes. However, the amplitudes of the asymmetric temperature perturbation fields from the TCDI–3DVAR and the conventional 3DVAR are very different. The former is quite close to the observed value and is 40%–60% greater than the latter.

4. TC intensity forecast with initial conditions from TCDI/3DVAR

In the previous section we show that the combined TCDI–3DVAR scheme is able to reproduce the observed MSLP, warm-core, and asymmetric circulation–temperature patterns while the conventional 3DVAR approach failed to do so. In this section, we use these two different sets of initial conditions and integrate the same model for 96 h. Note that the original simulation starts at $\tau = 0$ and is integrated to 144 h and the forecast fields at 48 h are used as the observed fields in our data assimilation experiment. In this forecast sensitivity experiment, the simulated fields from 48 to 144 h in the original continuous integration are used as the ''ground

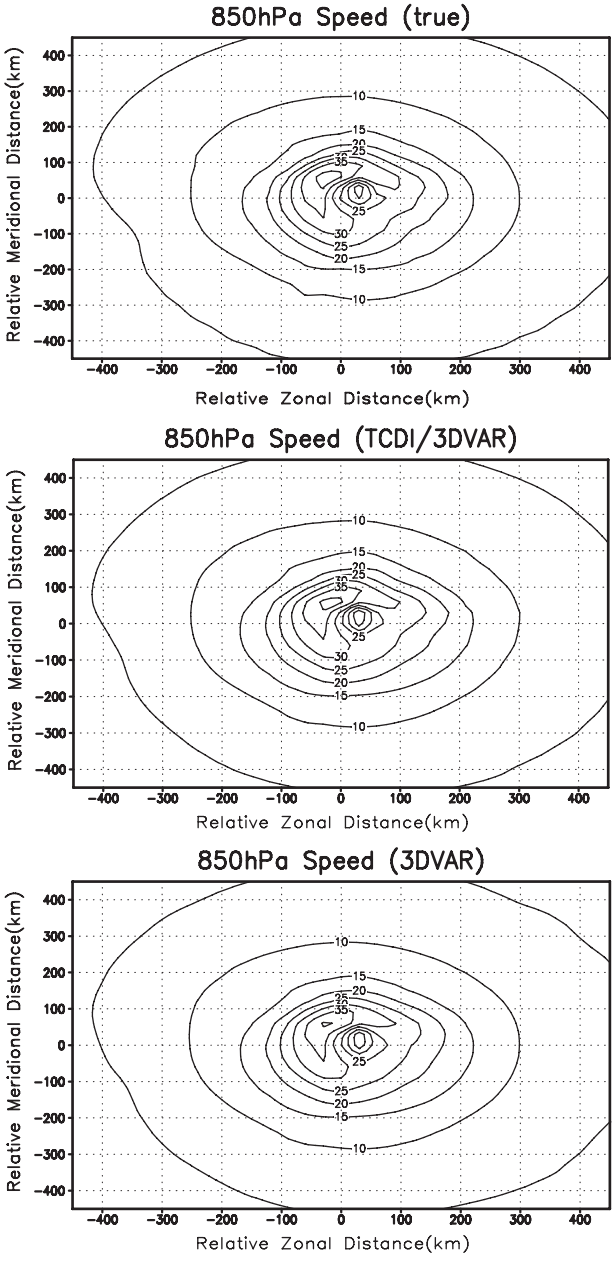

FIG. 7. (top) Observed wind speed field at 850 hPa, and the assimilated wind speed fields at 850 hPa from the (middle) TCDI–3DVAR and (bottom) conventional 3DVAR simulations.

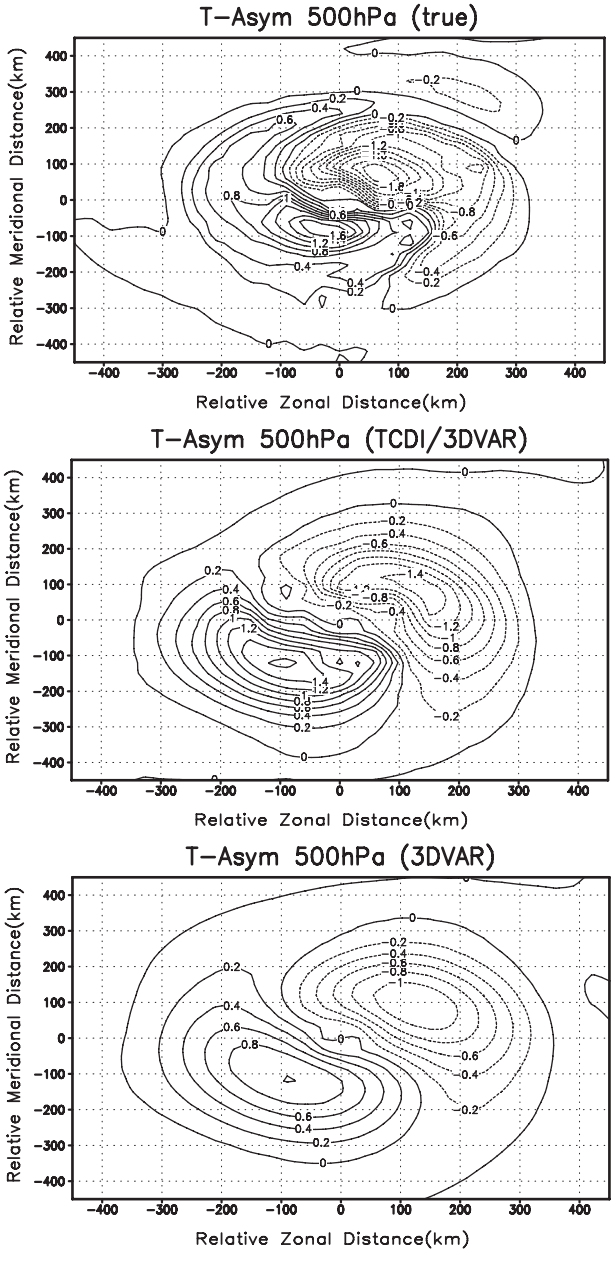

FIG. 8. (top) Observed asymmetric component of the 500-hPa temperature anomaly (K), and the assimilated asymmetric temperature fields from the (middle) TCDI–3DVAR and (bottom) conventional 3DVAR simulations.

truth'' for verification to see how differently an initial condition affects the subsequent prediction.

Figure 9 shows the three forecast results in comparison with the ground truth. The first experiment uses the weak Rankine vortex as the initial condition. As one can see, the initial intensity in the MSLP has a large error and remains separated from the ground truth throughout the integration even though the tendency is similar to the verification. The second experiment uses the initial conditions derived directly from the TCDI method (without the use of 3DVAR). As we can see, there is a large error at hour 96 (solid line) comparing with the observed TC MSLP. For the third experiment, the integration using the assimilation product from the TCDI–3DVAR scheme starts with the initial condition very close to the observed, and its subsequent integration (open-circle curve) follows the course of the verification (closed-circle curve). The

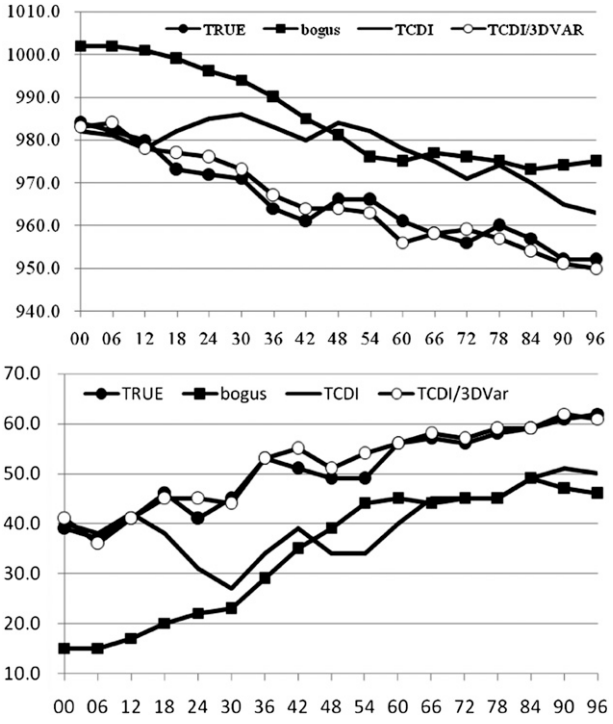

FIG. 9. The 96-h forecasts of the (top) TC MSLP (hPa) and (bottom) maximum wind speed at 850 hPa (m s^{-1}) with initial conditions from a weak Rankine vortex (closed square), the new TCDI–3DVAR initialization scheme (open circle), and the TCDI-only scheme (solid line). The observed pressure evolution from the OSSE is denoted by the closed-circle curves.

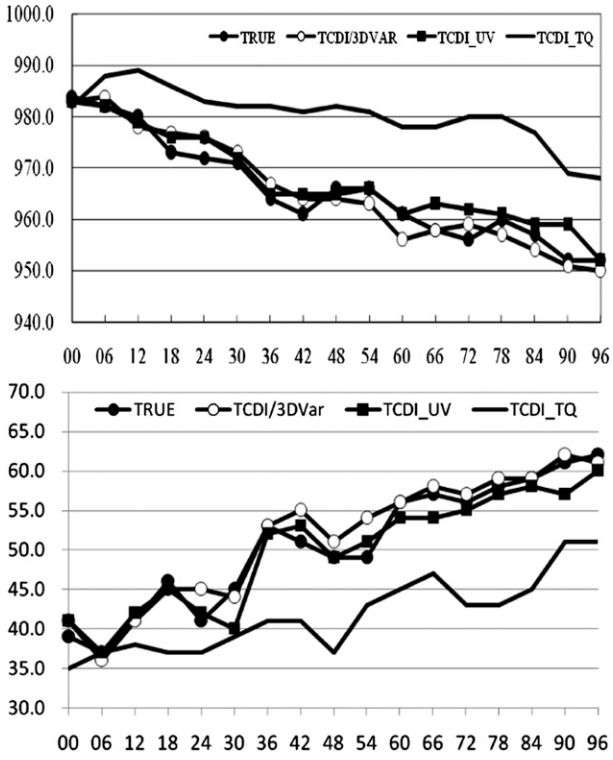

FIG. 10. The 96-h forecasts of the (top) TC MSLP (hPa) and (bottom) maximum wind speed at 850 hPa (m s^{-1}) with initial conditions from the TCDI–3DVAR (open circle), TCDI_TQ (solid line), and TCDI_UV (close square) simulations. The solid-circle curve denotes the observed evolution from the OSSE.

same assessment can be made for the prediction of the maximum wind speed at 850 hPa.

While all of the dynamic and thermodynamic fields are known in the idealized data assimilation experiment, not all atmosphere variables are available for assimilation in the real-world environment. For example, there is no complete 3D wind field for TCs. Questions remain as to the relative importance of the dynamic fields (such as 3D winds) and thermodynamic fields (such as 3D temperature and humidity) in TC initialization and intensity forecasts. To address these questions, we conducted two sets of idealized experiments. In the first experiment (TCDI_UV), only the observed 3D wind field and the MSLP information are given during the 3DVAR assimilation. In the second experiment (TCDI_TQ), only the observed 3D temperature and humidity fields and the MSLP information are known. The same first-guess field is used with the TCDI procedure that is used for the MSLP information.

Figure 10 shows the evolution of the forecasted MSLP and maximum wind speed at 850 hPa in the two new experiments. The forecasted MSLP and maximum wind speed in the TCDI_UV case are very close to the observed evolution, while there are large forecast errors in both the pressure and wind speed in the TCDI_TQ case, and the errors also increase rapidly with time. By the end of the integration, there is hardly any benefit from the combined TCDI–3DVAR scheme if only the MSLP–thermodynamic fields are assimilated. These sensitivity experiments suggest that the initial MSLP–wind observations play a more important role in the TC intensity forecasts than do the initial MSLP–temperature–humidity observations.

5. Discussion

a. Background error covariance and observation error covariance

As one can see from the results above, the conventional 3DVAR assimilation is capable of successfully retrieving the wind field in the OSSE but fails to recover the observed thermodynamic fields such as temperature, geopotential height, and surface pressure. As a result, there is a significantly large error in the initial TC intensity.

The advantage of the current 3DVAR-based dynamic initialization scheme is that after TCDI, a TC state with central minimum pressure much closer to the observed

state is obtained. Using this field as the first guess for 3DVAR, errors associated with the pressure-sigma vertical coordinate transfer in the TC core region are greatly reduced. As the 3DVAR quickly converges into an observed TC state, the nonlinear balance between the pressure and wind fields is kept valid to a large extent. Thus, in the current methodology, the TCDI prior to 3DVAR is a key factor that results in the improvement of the analysis of the initial TC state. The forecast experiments further demonstrate the feasibility of applying the new initialization scheme to operational TC forecast systems.

A possible cause of the conventional 3DVAR problem in the operational environment is the unrealistic representation of the BE. In the current study, to run the 3DVAR assimilation procedure, we simply took the default BE stored in the original WRF 3DVAR code. In current operational practice, the BE is generated based on a method developed at the National Meteorological Center (NMC; Parrish and Derber 1992), by assuming that the BE is static, flow independent, and isotropic. However, in the real atmosphere the BE may vary with time and space. A four-dimensional variational data assimilation (4DVAR) system or an ensemble Kalman filter (EnKF) system may provide a flow-dependent estimate of the BE, but because of the high computational cost, it is hard to use in a real-time operational environment. As an alternative, the proposed TCDI–3DVAR method may be easily implemented in operational TC forecast systems. As shown in Fig. 9, while there is significant error in the 24–96-h intensity forecast with the TCDI only, the combined TCDI–3DVAR methodology is capable of predicting a realistic intensity evolution, even though a default BE was applied. It is anticipated that the proposed TCDI–3DVAR initialization scheme with appropriate BE may further improve operational TC intensity forecast skills.

Another possible cause of the 3DVAR problem is attributed to the uncertainty in the observation error. There are several sources for the observation error, including those that are man made or from the equipment and nature, which are hard to eliminate. Usually, the observation error covariance matrix is assumed to be diagonal and constant. In our OSSE, we use the observation error covariance matrix stored in the original WRF 3DVAR code similar to the BE. It is likely that a more appropriate observational error covariance matrix may improve the TCDI–3DVAR assimilation results.

It is worth pointing out that the current OSSE study did not assume a zero observation error covariance; rather, we used an observation error covariance matrix stored in the original WRF 3DVAR code. Thus, even though the observed TC structure is given, there is an observation error associated with the observed data. We did include some level of reasonable observation noise.

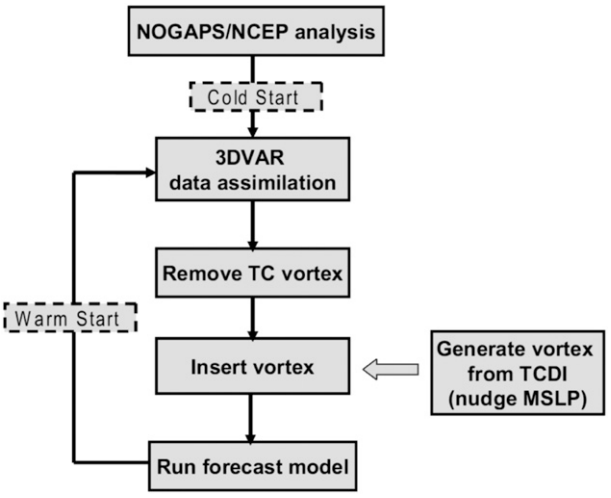

FIG. 11. Schematic of the COAMPS-TC initialization scheme (after Hendricks et al. 2011).

b. *Application of the TCDI–3DVAR scheme to an operational forecast system*

The aforementioned dynamic initialization scheme has been implemented in the Coupled Ocean–Atmosphere Mesoscale Prediction System for Tropical Cyclones (COAMPS-TC; Hendricks et al. 2011). Figure 11 is a flowchart describing how the TCDI approach is incorporated into COAMPS-TC. Note that the TCDI is applied to the COAMPS-TC analysis after 3DVAR is done, by simply removing the analysis fields in the TC surrounding region with TCDI-generated fields. The new scheme was tested in operational TC forecasts during the 2008 and 2009 hurricane seasons in both the North Atlantic and the western North Pacific basins.

As a case study, we examined the initialization and forecast of Hurricane Bill (2009). It is noted that the initial minimum central pressure using the TCDI is 955 hPa, which is consistent with the National Hurricane Center (NHC) best-track estimate, whereas it is only 979 hPa when using the standard 3DVAR system in the control experiment. The improvement in the initial conditions has a lasting effect on the subsequent evolution of the vortex. The TC 24–72-h intensity forecast using the new method is significantly better than that in the control experiment (see Fig. 6 of Hendricks et al. 2011). Because of the stronger TC intensity in the TCDI scheme, the forecasted rainfall pattern shows a more distinct eyewall structure, consistent with the TMI observations.

The COAMPS-TC 2008–09 forecast results indicate that the use of the new initialization procedure yielded significant improvements in the TC intensity forecasts. A comparison with an original scheme shows that both

the initial TC intensity and TC wind structure are improved. For example, mean absolute errors in the maximum sustained surface wind were reduced by approximately 5 kt for all lead times up to 72 h and mean absolute errors in the minimum central pressure were reduced by 10 hPa in the initial time and by about 5 hPa for all lead times up to 72 h (Fig. 9 of Hendricks et al. 2011).

6. Conclusions

In this study, through the observation system simulation experiment (OSSE) with the assistance of the WRF and its 3DVAR assimilation system, we demonstrate that even given the observed 3D TC fields as known, WRF 3DVAR failed to reproduce the observed MSLP and warm-core structure. A combined TC dynamic initialization (TCDI)–3DVAR scheme is proposed. The OSSE demonstrates that this new initialization scheme is capable of assimilating a TC 3D structure close to the ''observed.''

The specific procedure for the new initialization scheme may be summarized as follows. First, a first-guess vortex field derived from a global analysis will be spun up in a full-physics model in a quiescent environment. During the spinup period, the weak vortex is forced toward the observed MSLP in the presence of a 3D TC heating field. The final product is a balanced TC vortex with a realistic MSLP and warm core. This balanced TC vortex is then merged into the environmental field and used in the subsequent 3DVAR assimilation.

The application of the new initialization scheme leads to a much improved initial MSLP, warm-core, and asymmetric temperature patterns, compared to those from the conventional 3DVAR scheme. The forecast of TC intensity with the new initialization scheme is further conducted. The result shows that the model with the new initialization scheme is able to capture the observed intensity change, which leads to an improved intensity forecast. Further sensitivity experiments show that the initial 3D wind information seems more important than the initial temperature and humidity information in TC intensity forecasts.

The OSSE study above demonstrates the potential usefulness of the new TCDI–3DVAR scheme in operational applications. A preliminary application of the current scheme to COAMPS TC forecasts during 2008–09 summers was conducted and the results are encouraging. A further refining of the scheme to fit for operational use is currently on going, and the results will be reported upon in the near future.

Acknowledgments. This work was supported by the Special Project of the Chinese Academy of Meteorological Sciences (2007Y006), China National Science Foundation (Grants 40730948, 41075037), ONR Grant N000141010774, and by International Pacific Research Center that is partially sponsored by the Japan Agency for Marine-Earth Science and Technology (JAMSTEC), NASA (NNX07AG53G), and NOAA (NA17RJ1230).

REFERENCES

Barker, D. M., W. Huang, Y.-R. Guo, A. J. Bourgeois, and Q. N. Xiao, 2004a: A three-dimensional variational data assimilation system for MM5: Implementation and initial results. *Mon. Wea. Rev.,* **132,** 897–914.

——, M. S. Lee, Y.-R. Guo, W. Huang, Q. N. Xiao, and R. Rizvi, 2004b: WRF variational data assimilation development at NCAR. *Fifth WRF/14th MM5 Users' Workshop,* Boulder, CO, NCAR. [Available online at http://www.mmm.ucar.edu/mm5/workshop/ws04/Session5/dale.pdf.]

DeMaria, M., and J. Kaplan, 1999: An updated Statistical Hurricane Intensity Prediction Scheme (SHIP) for the Atlantic and eastern North Pacific basins. *Wea. Forecasting,* **14,** 326–337.

——, M. Mainelli, L. K. Shay, J. Knaff, and J. Kaplan, 2005: Further improvements to the Statistical Hurricane Intensity Forecasting Scheme (SHIPS). *Wea. Forecasting,* **20,** 531–543.

Hendricks, and Coauthors, 2011: Performance of a dynamic initialization scheme in the Coupled Ocean–Atmosphere Mesoscale Prediction System for Tropical Cyclones (COAMPS-TC). *Wea. Forecasting,* **26,** 650–663.

Holland, G. J., 1997: The maximum potential intensity of tropical cyclones. *J. Atmos. Sci.,* **54,** 2519–2541.

Hong, S.-Y., and H.-L. Pan, 1996: Nonlocal boundary layer vertical diffusion in a Medium-Range Forecast model. *Mon. Wea. Rev.,* **124,** 2322–2339.

——, Y. Noh, and J. Dudhia, 2006: A new vertical diffusion package with an explicit treatment of entrainment processes. *Mon. Wea. Rev.,* **134,** 2318–2341.

Kain, J. S., and J. M. Fritsch, 1993: Convective parameterization for mesoscale models: The Kain–Fritsch scheme. *The Representation of Cumulus Convection in Numerical Models, Meteor. Monogr.,* No. 46, Amer. Meteor. Soc., 165–170.

Knaff, J. A., C. R. Sampson, and M. DeMaria, 2005: An operational Statistical Typhoon Intensity Prediction Scheme for the western North Pacific. *Wea. Forecasting,* **20,** 688–699.

Kurihara, Y., M. A. Bender, and R. J. Ross, 1993: An initialization scheme of hurricane models by vortex specification. *Mon. Wea. Rev.,* **121,** 2030–2045.

Leslie, L. M., and G. J. Holland, 1995: On the bogusing of tropical cyclones in numerical models: A comparison of vortex profiles. *Meteor. Atmos. Phys.,* **56,** 101–110.

Lin, Y. L., R. D. Farley, and H. D. Orville, 1983: Bulk parameterization of the snow field in a cloud model. *J. Climate Appl. Meteor.,* **22,** 1065–1092.

McAdie, C., and M. B. Lawrence, 2000: Improvements in tropical cyclone track forecasting in the Atlantic basin, 1970–98. *Bull. Amer. Meteor. Soc.,* **81,** 989–997.

Michalakes, J., J. Dudhia, D. Gill, J. Klemp, and W. Skamarock, 1999: Design of a next generation regional weather research and forecast model. *Towards Teracomputing,* W. Zwieflhofer, Ed., World Scientific, 117–124.

Nuissier, O., R. F. Rogers, and F. Roux, 2005: A numerical simulation of Hurricane Bret on 22–23 August 1999 initialized with

airborne Doppler radar and dropsonde data. *Quart. J. Roy. Meteor. Soc.,* **131,** 155–194.

Parrish, D. F., and J. C. Derber, 1992: The National Meteorological Center's spectral statistical interpolation analysis system. *Mon. Wea. Rev.,* **120,** 1747–1763.

Skamarock, W. C., J. B. Klemp, J. Dudhia, D. O. Gill, D. M. Barker, W. Wang, and J. G. Powers, 2005: A description of the Advanced Research WRF version 2. NCAR Tech. Note NCAR/TN-468+STR, 88 pp.

Ueno, M., 1989: Operational bogussing and numerical prediction of typhoon in JMA. JMA/NDP Tech. Rep. 28, 48 pp.

Wang, Y., 2001: An explicit simulation of tropical cyclones with a triply nested movable mesh primitive equation model: TCM3. Part I: Model description and control experiment. *Mon. Wea. Rev.,* **129,** 1370–1394.

Xiao, Q., X. Zou, and B. Wang, 2000: Initialization and simulation of a landfalling hurricane using a variational bogus data assimilation scheme. *Mon. Wea. Rev.,* **128,** 2252–2269.

——, L. Chen, and X. Zhang, 2009: Evaluations of BDA scheme using the Advanced Research WRF (ARW) model. *J. Appl. Meteor. Climatol.,* **48,** 680–689.

Zhang, X., T. Li, F. Weng, C.-C. Wu, and L. Xu, 2007: Reanalysis of western Pacific typhoons in 2004 with multi-satellite observations. *Meteor. Atmos. Phys.,* 98, 3–18.

Zhou, X., and B. Wang, 2009: From concentric eyewall to annular hurricane: A numerical study with the cloud-resolved WRF model. *Geophys. Res. Lett.,* **36,** L03802, doi:10.1029/2008GL036854.

Zou, X., and Q. Xiao, 2000: Studies on the initialization and simulation of a mature hurricane using a variational bogus data assimilation scheme. *J. Atmos. Sci.,* **57,** 836–860.